8th International Symposium on Magnetic Bearing
August 26-28, 2002, Mito, Japan

SELF-SENSING CONTROL TECHNIQUE OF SELF-BEARING MOTOR

Toshiyuki Kurosu
Dept. of Mechanical Eng., Ibaraki University, Hitachi, Ibaraki-Pref., 316-8511 Japan
tkurosu@mech.ibaraki.ac.jp

Ken-ichi Matsuda
Dept. of Mechanical Eng., Ibaraki Univ., Hitachi, Ibaraki-Pref., 316-8511 Japan
matsu@mech.ibaraki.ac.jp

Yohji Okada
Dept. of Mechanical Eng., Ibaraki Univ., Hitachi, Ibaraki-Pref., 316-8511 Japan
okada@mech.ibaraki.ac.jp

ABSTRACT
This paper introduces a self-sensing technique of self-bearing motor by using the differential transformer principle. This self-sensing technique has wide linear range than the other system due to the use of the carrier frequency component. Therefore it is expected to have robust displacement information for the temperature fluctuation. Self-bearing motor uses P±2 pole algorithm which requires the two set of coils for the levitation and the motoring control. The opposed coil pair of the levitation is connected out of phase while that of motoring is connected in phase. Therefore it has the same structure of the differential transformer. Usually the motor is driven by the Pulse Width Modulated driving current. The induced carrier frequency component can be used for displacement estimation. In this paper, the fundamental principle is introduced how the self-sensing is achieved by the differential transformer principle. Then the differential output characteristics is examined experimentally. Finally the self-sensing levitation is carried out.

INTRODUCTION
In recent years, high speed and high efficient motor is required for high technological products. Contact type bearing is widely used to support the rotor. However, the mechanical contact causes several problems, such as friction and vibration. Furthermore maintenance and repairement are required. In order to solve these problems, magnetic bearings have been used which can support the rotor without physical contact. AC motor has good characteristics such as maintenance free, dustless and high efficiency. Therefore the rotor supported by magnetic bearing and driven by AC motor can rotate smoothly and achieve high speed rotation. However the length of the rotor increases causing low critical speed and bending vibration. The structure of magnetic bearing and AC motor are similar, hence self-bearing motor has been developed which has two functions of motor and magnetic bearing in a common rotor-stator pair. As a result, the total rotor system will be downsized and the critical speed can be increased [1].

Magnetic levitation system is always unstable, displacement sensor is required for feedback control to stabilize the self-bearing motor. The sensors are usually expensive and produce the non-collocation problem. The eddy current sensor is widely used which is affected by the actuator magnetic flux. The distance between the actuator and the sensor affects adversely to high frequency feedback stability. Hence several self-sensing techniques have been proposed to the magnetic levitation system. They are classified into two categories; observer based [2] and carrier frequency component ones [3]. The observer based type that estimates displacement from the relation between the control voltage and current has the advantage that it does not require any special hardware such as filter and demodulation circuit. However it cannot estimate the static displacement. On the contrary, the carrier frequency type requires a special hardware to detect the inductance difference caused by the airgap change in the electromagnetic circuit. The advantage is that it can estimate the real displacement. However, the estimated displacement from only the actuator inductance does not have wide linear range and is influenced by the temperature. In order to improve these problems, we proposed a differential transformer (DFT) type dis-

placement estimation. The airgap of the magnetic bearing has been successfully estimated [4]. In this paper, the DFT type self-sensing technique is applied to the self-bearing motor.

PRINCIPLE OF LEVITATION AND ROTATION

The P±2 type self-bearing motor has been developed and applied to the PM type, induction type, and reluctance type motors [5]. Due to the high efficiency and low temperature rise only PM type motor is applicable to the hard disk drive and artificial heart pump. Therefore the PM type motor is considered in this paper. The principle of rotation and levitation for the PM type motor is summarized.

The rotor with an M pole pair number is assumed to produce the following flux density:

$$B_r(\theta,t) = B_R \cos(\omega t - M\theta) \tag{1}$$

where B_r = peak density of magnetic flux, ω = motoring frequency, and θ = angular coordinate (assumed zero at y direction).

A current sheet of the stator is assumed to have the following current distribution to produce the rotating torque:

$$I_m(\theta,t) = -I_M \cos(\omega t - M\theta - \phi) \tag{2}$$

where I_M = the peak current, and ϕ = the phase difference.

Therefore the rotating torque is calculated as following equation using Flemming's left hand law:

$$\begin{aligned} T &= r\int_0^{2\pi} B_r(\theta,t) I_m(\theta,t) L d\theta \\ &= B_R I_M r L \pi \cos\phi \end{aligned} \tag{3}$$

where r = radius of rotor, and L = effective length of windings. Therefore, the motoring control is achieve by changing the phase of motoring current ϕ.

Next, the levitation control is considered. Let us consider the N pole pair current in the stator which gives the following magnetic flux:

$$\begin{aligned} B_f(\theta,t) = &-B_{F1}\cos(\omega t - N\theta) \\ &-B_{F2}\sin(\omega t - N\theta) \end{aligned} \tag{4}$$

where B_{F1} and B_{F2} are the peak densities of two components of flux distribution. Then the total magnetic flux density in the airgap is given as the following equation.

$$B = B_r(\theta,t) - B_f(\theta,t) \tag{5}$$

This flux produces the attractive force in θ direction.

$$\Delta F(\theta) = \frac{B^2}{2\mu_0}\Delta S \tag{6}$$

where ΔS is the infinitesimal area. Hence the total levitaion force in $\theta = 0$ direction is given by

$$\begin{aligned} F_y &= \int_0^{2\pi}\int_0^L \Delta F(\theta) r\cos\theta \\ &= \frac{B_R B_{F1} r L}{4\mu_0}\int_0^{2\pi} [\cos\{(M-N-1)\theta\} \\ &\quad + \cos\{(M-N+1)\theta\}] d\theta \end{aligned} \tag{7}$$

where L = length of rotor, μ_0 = permeability of free space.

The equation becomes a constant force

$$F_y = \frac{\pi B_R r L}{2\mu_0} B_{F_1} \tag{8}$$

when $M - N = \pm 1$. That is, a pure levitation force can be obtained when the stator pole number = the rotor pole number $\pm$ 2.

The x directional force is calculated by integrating the x component of (6) as the following,

$$F_x = \frac{\pi B_R r L}{2\mu_0} B_{F_2} \tag{9}$$

Hence, two-dimensional radial position of the rotor can be controlled by changing the magnitude of B_{F1} and B_{F2}.

PRINCIPLE OF SELF-SENSING

This paper introduces a self-sensing technique of self-bearing motor by using DFT principle. In this section, the displacement output characteristics is examined theoretically. Then the possibility of self-sensing control for self-bearing motor is considered.

The schematic of the DFT is shown in Figure 1. The DFT consists of reference coil, two output coils, and the iron core. The reference coil is driven by AC current of the constant frequency, which produces the flux crossing to the output coils. The voltage of e_{x1} and e_{x2} is induced in the output coils. The difference $e_{x1} - e_{x2}$ is used for estimation, because the upper and lower output coils are connected reversely. Therefore if the iron core is at the center, the differential output is zero. This characteristics is shown in the right side of Figure 1.

The arrangement of the levitation and the motoring coils of the self-bearing motor is shown in Figure 2. The self-bearing motor requires two sets of coils; one is the motoring and another is the levitation coils. The levitation coils are always reversely

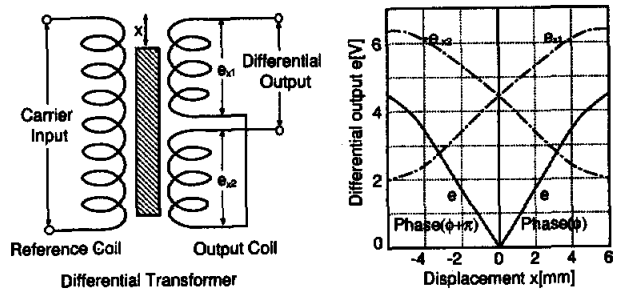

FIGURE 1: Principle of Differential Transformer

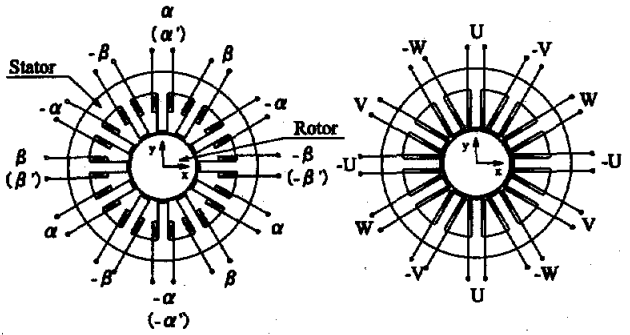

FIGURE 2: Arrangement of Levitation and Motoring Coils

connected between the opposite poles. This structure is the same of the DFT type displacement sensor. When the motoring coils are driven by a pulse width modulated (PWM) 3 phase current, the PWM carrier frequency component is induced in the levitation coils, which is expected to be linear to the rotor displacement. The current is measured by the resistance voltage connected series to the coil.

Next let us consider the mutual inductance and the characteristics of the displacement information. Assuming that the magnetomotive force $F_U(\theta)$ caused by the unit current of U phase coils is the sinusoidal form as

$$F_U(\theta) = F_0 \cos 2\theta \tag{10}$$

Similarly, the magnetomotive forces $F_\alpha(\theta)$ and $F_\beta(\theta)$ caused by the unit current of α and β phase coils are given by

$$\begin{aligned} F_\alpha(\theta) &= F_1 \cos 3\theta \\ F_\beta(\theta) &= F_1 \sin 3\theta \end{aligned} \tag{11}$$

The permeance dP_{eq} of an infinitesimal part between the rotor and the stator is given by

$$dP_{eq} = \frac{\mu_0 r w (l_0 - x\sin\theta + y\cos\theta)}{l_0^2} d\theta \tag{12}$$

where r = the radius of the rotor, w = the thickness of the rotor, l_0 = airgap, x and y the displacement in x and y directions. Furthermore, the interlinkage fluxies between U phase coil and α, β phase coils are given by

$$\begin{aligned} d\psi_{U_\alpha} &= F_U(\theta) F_\alpha(\theta) dP_{eq} \\ d\psi_{U_\beta} &= F_U(\theta) F_\beta(\theta) dP_{eq} \end{aligned} \tag{13}$$

Therefore mutual inductance $M_{U_\alpha}, M_{U_\beta}$ are given as the following equations.

$$M_{U_\alpha} = \int_0^{2\pi} F_U(\theta) F_\alpha(\theta) dP_{eq} = \frac{F_0 F_1 \mu_0 r w \pi}{2 l_0^2} y \tag{14}$$

$$M_{U_\beta} = \int_0^{2\pi} F_U(\theta) F_\beta(\theta) dP_{eq} = -\frac{F_0 F_1 \mu_0 r w \pi}{2 l_0^2} x \tag{15}$$

From this result, M_{U_α} changes according to y displacement while M_{U_β} changes according to x displacement. Therefore it is possible to estimate the displacement x, y based on the high frequency voltage in α, β coils respectively.

Let α', β' be the part of coils of α, β which are wound only on U phase. Then magnemotive force $F_{\alpha'}(\theta)$ and $F_{\beta'}(\theta)$ are expressed as the following equation using Dirac's delta function.

$$F_{\alpha'} = F_1[\delta(\theta) + \delta(\theta - \pi)] \tag{16}$$

$$F_{\beta'} = F_1[\delta(\theta - \frac{\pi}{2}) + \delta(\theta + \frac{\pi}{2})] \tag{17}$$

Therefore mutual inductance $M_{U\alpha', U\beta'}$ is calculated as

$$M_{U\alpha'} = 2\mu_0 \frac{F_0 F_1 \mu_0 S}{l_0^2} y \tag{18}$$

$$M_{U\beta'} = 2\mu_0 \frac{F_0 F_1 \mu_0 S}{l_0^2} x \tag{19}$$

where S is the area of slot. From equations (18) and (19) it is possible to estimate the displacement of x, y directions by using the induced voltage in α', β' coils.

EXPERIMENTAL RESULTS AND CONSIDERATIONS

The schematic of the experimental setup is shown in Figure 3. This motor is the inner rotor type. The rotor is set vertically. The upper end is supported by the ball bearing. Hence it has two radial degrees of freedom. The airgap between the rotor and stator is 1.0 mm. The touchdown plate is used to prevent the rotor from directly contact. Then the movable gap is 0.4 mm. Two gap sensors are used to monitor the real displacements.

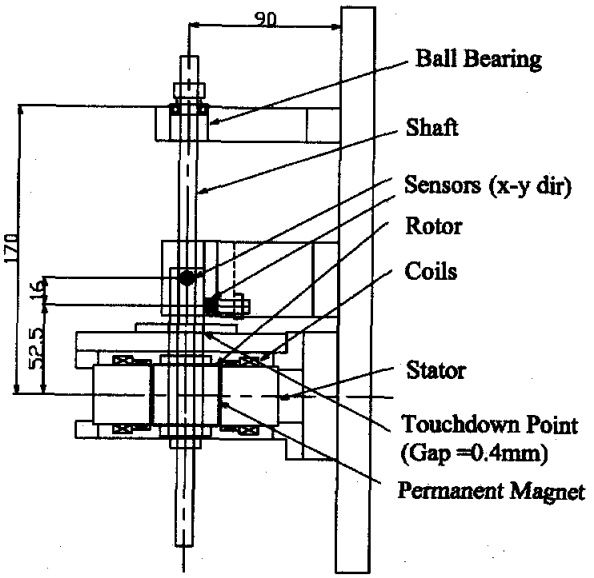

FIGURE 3: Schematic of Experimental Setup

The system is designed using the finite element code ANSYS. It is confirmed that the magnetic flux in the stem of the stator is under the saturation level when the airgap is 1.0 mm and thickness of permanent magnet is 0.7 mm . The rotor is made of laminated steel sheet. Four permanent magnets are glued N poles and S poles alternatively on the surface of the rotor. The magnets are diamond shaped to have the smooth sinusoidal flux in the airgap. The stator is also made of the laminated steel sheets. Two sets of coils for the levitation and rotation are inserted in the slot of the stator. The opposed levitation coils are connected out of phase, while the rotation coils are connected in phase. This motor is the 4 pole PM type. The levitation is controlled by using 3 phase 4 pole motoring current, while the levitation is controlled by 2 phase 6 pole levitation current separately.

Control System

The estimation is carried out by using the detection circuits shown in Figure 4. The U phase of rotation coils is driven by PWM signal of the frequency of 10 kHz. Then the carrier components of the current induced in α', β' phase coils are measured. The carrier component is filtered using the band path filter and put into the analog multiplier. Then, it is sent to a low pass filter to remove the carrier frequency component. This demodulated signal is expected to be linear to the displacement of the rotor.

The control system is shown in Figure 5. The digital signal processor DSP(dSPACE DS1104) is used for rotation and levitation control. Levitation control used is the standard digital PID controller. First,

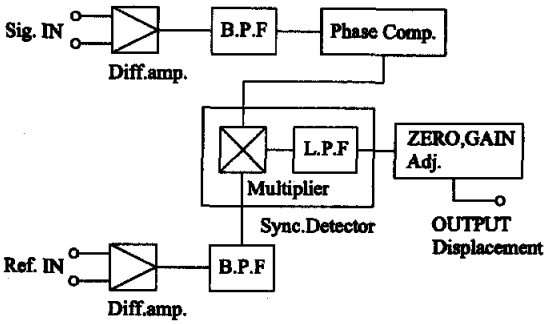

FIGURE 4: Detection Circuit

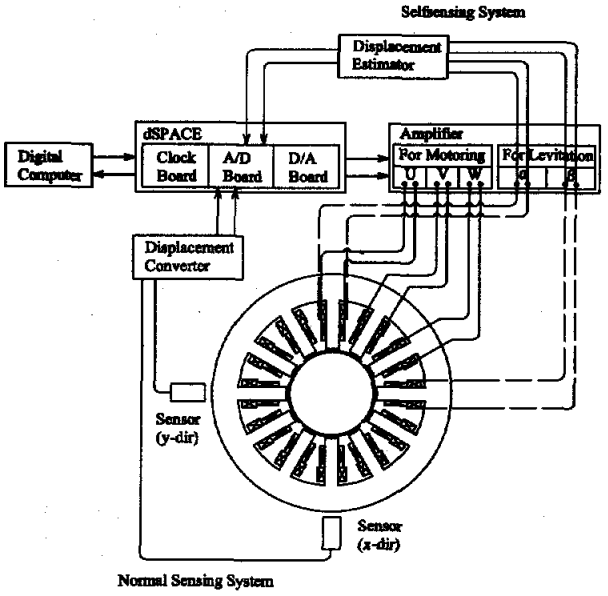

FIGURE 5: Control System

the displacement of the rotor is measured and put into DSP through A/D converter. The actuating signal is calculated in DSP from the displacement signal and put out to the power amplifier. The supply voltage used is ± 35 V.

Static Estimation

To confirm the estimation accuracy static estimation is carried out. The results are shown in Figures 6 to 9. Figure 6 shows the estimated displacement of x when the rotor angle is 0°. The results are almost linear to the displacement x, but it fluctuates according to the levitation current. However the estimation is very accurate when the rotor angle is $\frac{\pi}{4}$ as shown in Figure 7 due to the absence of permanent magnet. Figures 8 and 9 show similar results in y direction. These results show that the displacement estimation is possible, but it is affected by the angular position of the rotor and the levitation current.

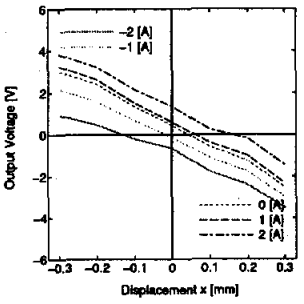

FIGURE 6: Characteristics of Displacement Estimation (x direction, $\omega t = 0$)

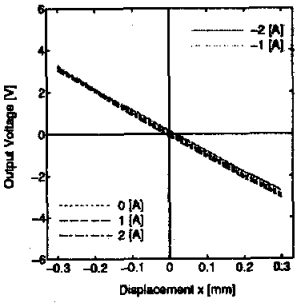

FIGURE 7: Characteristics of Displacement Estimation (x direction, $\omega t = \frac{\pi}{4}$)

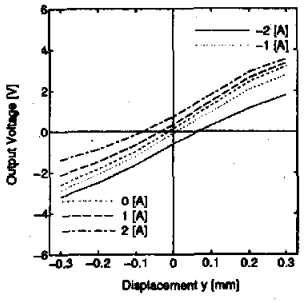

FIGURE 8: Characteristics of Displacement Estimation (y direction, $\omega t = 0$)

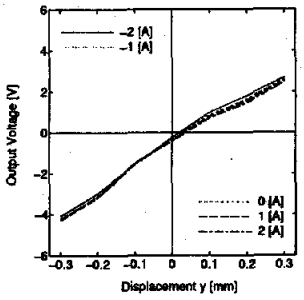

FIGURE 9: Characteristics of Displacement Estimation (y direction, $\omega t = \frac{\pi}{4}$)

Dynamic Estimation

The dynamic estimation is carried out by levitating the rotor with the sensor displacement and recording the impulse response on y direction as shown in Figures 10 and 11. The results on x direction are very similar to those on y direction. Hence only y directional results are shown. Figure 10 is the results when the rotor position is 0° while Figure 11 is that of $\frac{\pi}{4}$. In both cases the upper curve is the measured displacements while the lower is the estimated ones. The self-sensing output agrees relatively well with the sensor output. However the self-sensing output includes vibrating fluctuation. The reason is the noise output causing by the levitation current.

Self-Sensing Levitation

In this section, the levitation control by self-sensing signal is carried out. The sensor and the estimated signals are measured and compared. Figures 12 and 13 show the impulse responses by hammering the rotor causing about 0.1 mm displacement and recording the decaying vibration. The y directional results are shown in Figures 12 and 13. Figure 12 shows the results when the rotor angle is 0° while figure 13 is the results when the rotor angle is $\frac{\pi}{4}$. The estimated signal in the lower graph includes higher noise but is well agreed with the measured upper signal. The response controlled by the estimated signal show good

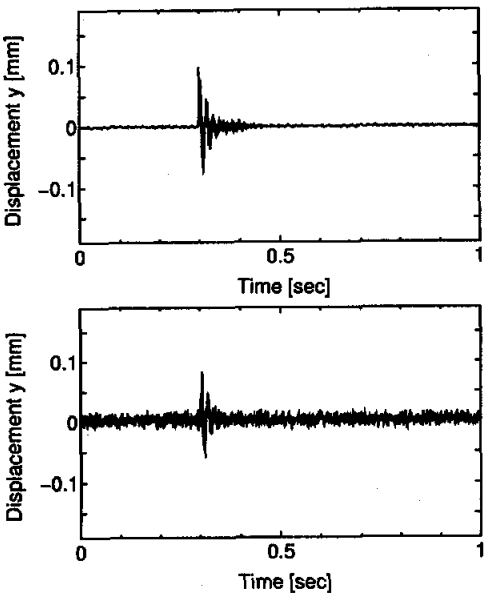

FIGURE 10: Impulse Response for y direction with Sensor Control, $\omega t = 0$ (Sensor Output (Upper), Self-Sensing Output (Lower))

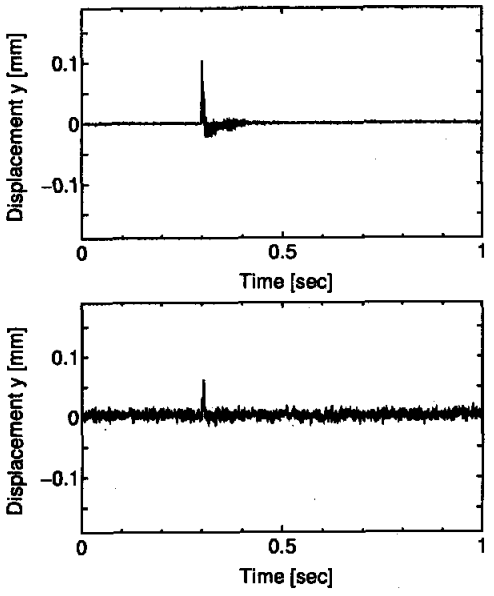

FIGURE 11: Impulse Response for y direction with Sensor Control, $\omega t = \frac{\pi}{4}$ (Sensor Output (Upper), Self Sensing Output (Lower))

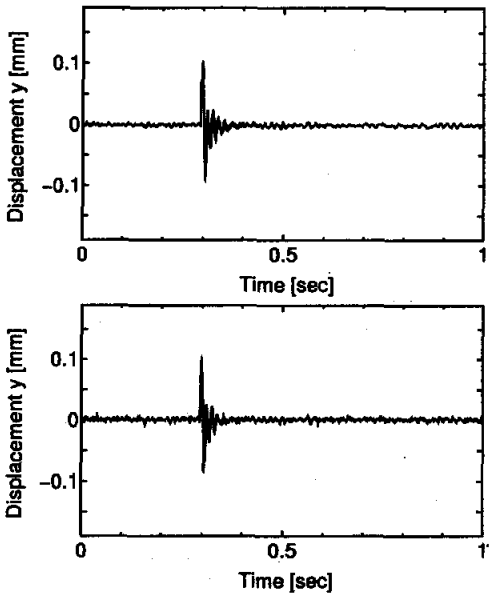

FIGURE 12: Impulse Response for y direction with Self-Sensing Control, $\omega t = 0$ (Sensor Output (Upper), Self-Sensing Output (Lower))

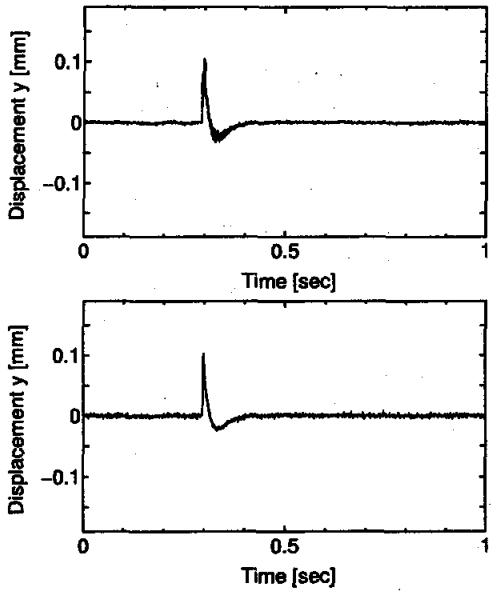

FIGURE 13: Impulse Response for y direction with Self-Sensing Control, $\omega t = \frac{\pi}{4}$ (Sensor Output (Upper), Self-Sensing Output (Lower))

damping which is considered due to the collocated arragement. This is one of the good point of self-sensing technique. However the self-sensing signal includes the fluctuation according to the rotor position and current. Hence we could not achieve the levitated rotation by the self-sensing control.

CONCLUSION

In this paper, the self-sensing technique of the self-bearing motor is proposed. The displacement estimation and levitation are carried out. The estimated signal includes the linear signal to the rotor displacement. The static levitation was succeeded, but the rotor could not rotate. This is due to the fluctuation caused by the rotor angular position and driving current. Further work is continuing to get accurate self-sensing signal and successfully levitated rotation with the self-sensing signal.

References

1. Okada, Y., et. al., Levitation Control of Permanent Magnet (PM) Type Rotating Motor, Proc. of Magnetic Bearings, Magnetic Drives and Dry Gas Seals Conf. Exhibition, July 29-31, 1992, Alexandria, Va, USA, pp.157-167

2. Vischer. D. and Bleuler. H., A New Approach to Sensorless and Voltage Controlled AMBs Based on Network Theory Concepts, 2nd International Symposium on Magnetic Bearings, July 12-14, 1990, Tokyo, Japan, pp.301-306

3. Noh. D. M. and Maslen. H. E., Self-Sensing Magnetic Bearings (Part I), Fifth International Symposium on Magnetic Bearings, August, 1996, Kanazawa, Japan, pp.95-100

4. Matsuda, K., et. al., Self-sensing Magnetic Bearing using the Principle of Differential Transformer, Fifth International Symposium on Magnetic Bearings, August, 1996, Kanazawa, Japan, pp.107-112

5. Okada, Y., et. al., Analysis and Comparison of PM Synchronous Motor and Induction Motor Type Magnetic Bearing, IEEE Transactions on Industry Applications, Vol.31, No.5, September/October, 1995, pp.1047-1053